frontiers | Frontiers in Environmental Science

TYPE Original Research
PUBLISHED 12 March 2025
DOI 10.3389/fenvs.2024.1494730

OPEN ACCESS

EDITED BY
Paweł Tomczyk,
Wroclaw University of Environmental and Life Sciences, Poland

REVIEWED BY
Qingguang Li,
Guizhou University, China
Mohamed Gad,
University of Sadat City, Egypt

*CORRESPONDENCE
Qiao Xiaojuan,
qiaoxj2010@163.com
Liu Kai,
acancer@163.com

RECEIVED 11 September 2024
ACCEPTED 18 November 2024
PUBLISHED 12 March 2025

CITATION
Xiaojuan Q, Baoling L, Kai L, Xinyu C and Wenjin Y (2025) Hydrochemical characteristic and karst development in typical karst spring area, Northern China.
Front. Environ. Sci. 12:1494730.
doi: 10.3389/fenvs.2024.1494730

Hydrochemical characteristic and karst development in typical karst spring area, Northern China

Qiao Xiaojuan[1,2]*, Li Baoling[3], Liu Kai[4]*, Chai Xinyu[1] and Yu Wenjin[1]

[1]College of Earth and Planetary Sciences, University of Chinese Academy of Sciences, Beijing, China, [2]Key Laboratory of Earth System Numerical Modeling and Application, Chinese Academy of Sciences, Beijing, China, [3]Sino-Danish College, University of Chinese Academy of Sciences, Beijing, China, [4]Chinese Academy of Geological Sciences, Beijing, China

Karst aquifer is controlled by complex tectonics. While the tectonic effects and its relationship with chemical evolution in large-scale karst areas are always be neglected. This study focuses on the relationship and systematically analyzed structure control on hydrochemical indicators for karst development in Fangshan, Beijing, North China. The results show that the hydrochemical type changes from mainly HCO_3-Ca·Mg, HCO_3-SO_4^{2-}-Ca·Mg, to HCO_3-Mg·Ca along with the flow. The ions relationship, Gibs and SI analysis show the process is mainly rock weathering. From recharge to the discharge area, the increases of Mg^{2+} mainly due to dedolomitization process and the desulfation results in sulfate reduction. Total dissolved solid (TDS) increases from 261 to 630 mg/L along the flow. While, its core around the fracture-intensive zone is low (less than 247 mg/L). And higher Sr concentration neighboring lamprophyre (χ) and magmatic rock (γ). It proved that the overprint of two-episodic tectonism processes caused a series of NE-NW fold-back thrust nappe structures and a number of faults intersection areas, effects hydrochemical characteristic. The direction of a series of karst caves is consistent with the direction of the Xiayunling fold-back thrust nappe structure indicates that multi-stage tectonic activity creates runoff channels and WRI space and impact cave distribution. Our work is benefit to understanding the role of fractures on karst development from the perspective of hydrochemical view in the groundwater flow, which can provide a basis for further formulating the planning of karst water exploitation.

KEYWORDS

hydrochemistry, karst groundwater, water-rock interaction, tectonic fracture, North China

1 Introduction

Groundwater in karst aquifers are very important resource, at least a partial source of drinking water supply to almost 25% of the world's population (Kollarits et al., 2006; Ford and Williams, 2007; Andreo et al., 2008). Approximately 10% of the world's land surface areas have karst aquifer beneath them, which usually are evolved from fractured or fractured-porous rock networks after several years through carbonate dissolution creating large passages and caves (Koosha, 2019). While, the degree of karst aquifer is influenced by various factors. Geological structure (e.g., fractures and faults), lithology (carbonate rock thickness, mineral chemical composition),climate (temperature, type and amount of precipitation), hydrology condition (flow field, hydrochemical

characteristic),topography and vegetation, etc. are the most important factors in determining the degree of karst development (White, 1988; Benischke et al., 2007).

Previous studies around the karst development topic focused on the influence of climate on karstification using various geological investigation methods, such as geophysical electromagnetic or seismic methods (Benischke et al., 2007; Winter et al., 1991; Nativ et al., 1999; Laskow et al., 2011; Illman and Neuman, 2001; Boucher et al., 2006) or various models, for the depiction of karst conduit evolution (Dreybrodt et al., 2005; Florea, 2015; Shu et al., 2020), and discuss the water–rock interaction between groundwater and the mineral facies of aquifers using chemistry and isotopes method (Ledesma-Ruiz et al., 2015; Gil-Marquez et al., 2017; Mohamed and Ahmed, 2017; Shen, 1993; Pu et al., 2013; Zang et al., 2013; Cartwright et al., 2012; Marques et al., 2013; Gil-Márqueza et al., 2020). Although some scholars have discussed the control function of geological structure (Valdes et al., 2007; Wang and Jia, 2007) on karst groundwater. Due to the heterogeneity of karst media (Ni et al., 2009), the complexity of the fissure network, and the diversity of influencing factors, the control function of geological structure (Dong et al., 2014; Qiao et al., 2014; Xie et al., 2007) on karst groundwater system needs to be further studied (Wan et al., 2010). Especially, for the fissure-karst water-bearing system in North China, erosion fissure is the most common karst form, and it is also the main channel of groundwater recharge, storage and flow. Therefore, the main controlling factor of karst development is geological structure and groundwater flow field in the fissure-karst water system. However, the work analyzing the hydrochemical evolution and karst through combing the distribution of geological fracture network with the groundwater recharge, runoff, discharge, distribution is limited. The aim of our research is revealing the systematic relationship of hydrochemical characteristic and karst development from the viewpoint of groundwater flow concept.

The distribution area of carbonate reaches 4,900 km^2 in Beijing, North China. Fangshan karst area is located in the Western Hills of Beijing, wherein the intersection of the Taihang and Yanshan tectonic belts is special enough. Groundwater is characterized in this study by abundant resources and good water quality. The emergency water source site of Zhangfang provides drinking water to more than a million people (Li, 2012). Many institutions and researchers have conducted numerous investigations in recent years in the Fangshan area, including joint and fracture characteristics, hydrogeochemical characteristics, current exploitation situation, geological structure evolution, distribution of karst cave system formation, and interaction between groundwater and surface water in karst groundwater systems (Chu et al., 2017; Bi, 1986; Cao et al., 2014; Dong et al., 2014; Guo et al., 2011; Lv et al., 2010; Qiao et al., 2014; Wang et al., 2016; Xin, 2005; Yang et al., 2014). Although, some basic data has been accumulated for many years of investigation of Beijing Fangshan karst development area. However, due to the complexity of the karst fissure network space distribution and the heterogeneity of karst groundwater distribution, the previous investigations on a systematic and regional fracture network and the geochemical evolution of groundwater are limited. In particular, occurrence rules and tectonic control function in Fangshan area of Beijing is still very weak, which hampers sustainable management of regional water resources. (Lv et al., 1999; 2010; Ye et al., 2005; Guo et al., 2011).

Therefore, this study aims to consider the viewpoint from hydrogeochemical evolution processes in flow field under the complex geological fracture environment in Zhangfang, Fangshan areas, and we will perform the following work: (i) analyze hydrogeochemical characteristic and caves distribution through possible water–rock interaction analysis; (ii) evaluate the regulation and influence of the of the karst–fracture network system on hydrogeochemistry. (iii) document the possible dominant geochemical processes with the groundwater recharge, runoff, discharge direction.

Through the study of karst development characteristics and water chemical evolution process, the mechanism of karst development and karst water occurrence characteristics in Fangshan area can be revealed, which provides a basis for further formulating the planning of karst water exploitation and utilization and the target area of karst water exploration in Beijing. The karst geomorphology in this area is a typical representative of karst in North China and there are many other karst areas with similar conditions. Therefore, this work is of instructive significance and has practical value in other similar areas of North China.

2 Study area

2.1 Site and climate

The study area is located in the southwest part of the Fangshan District in Beijing, occupying a total area of approximately 500 km^2, which is the transition zone between the North China Plain and the Taihang Mountains (Figure 1). The topography is dominated by mountainous areas and affected by the Juma River. The area is also lower in the east and south than in the west and north between longitudes 115°15′and 116°10′E and latitudes 39°00′and 39°90′N. Moreover, the study area belongs to the continental monsoon climate, and its annual temperature varies from the maximum value of 40 °C in July to a minimum value of −22°C in January. According to meteorological data (1978–2014) from the Fangshan weather station (Figure 2), the mean annual rainfall is 574 mm, and the variation of annual rainfall ranges from the maximum value of 924.8 mm in 1996 to a minimum value of 324.1 mm in 2006. The mean potential evaporation is around 1,500 mm. The atmospheric precipitation accounts for approximately 85% of yearly rainfall from June to September.

2.2 Geological setting and hydrogeological condition

Karst groundwater in the Fangshan district is divided into several major hydrogeological units. This research focuses on Xiayunling–Longmentai synclinorium hydrogeological unit, which is the emergency water source located in Zhangfang, as shown in Figure 1. In this hydrogeological unit, the outcropping strata, including Jixian system (Jxw, Jxh, Jxt), Neo-Proterozoic Qingbaikou system (Qn), Paleozoic Cambrian-Ordovician (Ꞓ-O), Carboniferous-Permian (C-P), and Mesozoic Jurassic–Cretaceous (J-K), are relatively complete. The carbonate strata of outcrops mainly include siliceous dolomites, dolomitic limestone, sandy dolomite, argillaceous dolomite, shale, and silty sandstone. The

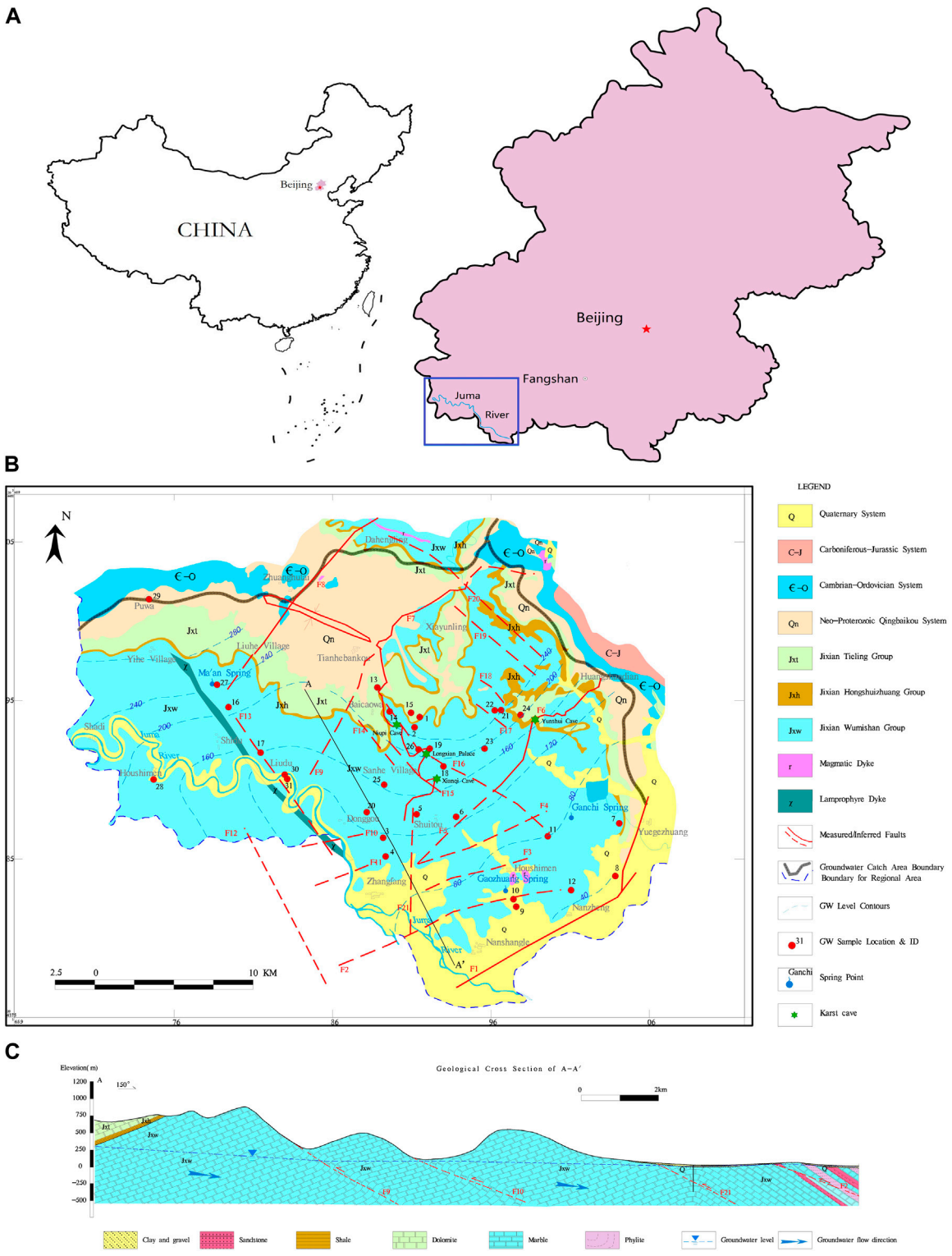

FIGURE 1
Location, topography map, and hydrogeological map of Fangshan, China. **(A)** Location and topography of the study area. **(B)** Hydrogeological map and sampling site distribution. **(C)** Hydrogeological cross-section (A-A′).

majority of strata is dolomite of the upper Proterozoic, followed by limestone of the lower Paleozoic. These marine sedimentations, which contain calcium carbonate, magnesium, and small amounts of silica and iron, produced folds and fractures due to repeated crustal movements, especially tectonic movements in the Mesozoic and Cenozoic ages. Lamprophyre dyke (χ) outcrop is found along the

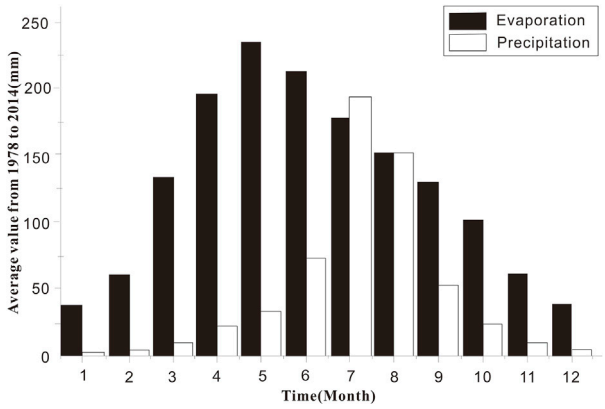

FIGURE 2
The average value of monthly precipitation and evaporation from 1978 to 2014 at Fangshan station.

Zhangfang-Ma'an village. Several groups of faults, including the N-E (F1–F11), N-W (F12–F20), and S-N (F21, namely Dayugou fracture) groups, are developed in this region (Figure 1). Thereinto, large-scale thrust nappe structures (F1, F6, F7, F8), which crosscut Xiayunling–Longmentai synclinorium and formed multistage overthrust faults, are well developed.

The aquifers comprise the porous Quaternary sediments and carbonate karst aquifers in the study area. For the Quaternary aquifer, it is mainly distributed in the southeastern part of the hill, mountain valley, and Piedmont plain. This aquifer comprises silty sand on the surface and gravel in the lower part of the layer with a thickness of less than 20 m. While, the main the groundwater type here is mainly karst-fissure groundwater. The recharge in this region is mainly due to the precipitation infiltration, river drainage, and irrigation recharge. Fractures developed on rock surfaces have good infiltration conditions. Precipitation recharge in the rainy season considerably increases the groundwater level. The discharge, especially the seepage from Zhangfang downstream, occurs along the Juma River channel.

Groundwater runoff is complex because of fractures, which are crucial in controlling the distribution and flow of groundwater, as shown in Figure 1. Niukouyu–Changgou (F1), Huangshandian (F6), Xiayunling (F7), and Zhuanghutai (F8) faults are regional large-scale faults in this area. These fractures are generally tilted south-east and stretched for scores of kilometers. The accompanying and communicating transverse fissures also help groundwater migration from northwest to southeast, while some of the structures act as water traps. For example, the existence of Shimen intrusive rock (γ), sandstone, and phyllite leads to the discontinuity of karst fissures and changes in groundwater runoff. Groundwater meets fractures with low permeability and eventually creates the springs. Another example is along the area of Gaozhuang village, where the thick layer of marble, sandstone, and phyllite distributed along the south of F2 forms a weak permeable formation. This layer hinders the runoff of groundwater to the south. The magmatic rock (γ) mass is exposed to Shimen village and has a distribution area of around 1 km^2. The lithology of this rock is granodiorite, which blocks the runoff of groundwater to the east. Gaozhuang and Ganchi springs outcrop in front of a mountain because of the blocking rock or fracture, as shown below in Figure 3.

The discharge includes the base flow, spring discharge, and artificial exploitation (Chu et al., 2017). The curve of quantity change in Gaozhuang and Ganchi springs from 2003 to 2013 is shown in Figure 4. The flow fluctuation of the two springs is very different. It may indicate that they are two independent spring areas and the magmatic rock (γ) mass plays impenetrable structure.

3 Investigation and testing

3.1 Investigation in the field

This area experienced multiple tectonic periods, including the Pre-Indochina period, the Indochina period, Stage of Yanshan, and Himalayan period, and generated fold and joint structures in different directions during movements.

The structure of the Indo-branch period occurs in the late middle Triassic to the late Triassic. The main stress is the north-south extrusion, and the east-west cloth in the research area. The Yanshanian movement occurred from the late Jurassic to the late Cretaceous, and the force was the north-south-east extrusion contraction and the counterclockwise twist in the north-south direction. The Himalayan movement occurred from the late Cretaceous to the present, with the north-south-east tension stretching and the north-south direction of clockwise twisting.

From the perspective of tectonic evolution, the Jurassic thrust fault and related folds indicate that the environment is in an extrusion state, with more water resistance fracture structures, such as f1 (thrust nappe structure); the Cretaceous evolved into an extended structural environment, and the structure mainly moves again along the early tectonic weak zone, making the extrusion fracture tension more broken and forming a high-angle positive fault (f2 is extension structure) as shown in Figure 5. The geological fracture underwent two-episodic tectonism, which is thrusting nappe structure in the Jurassic period and extensional structure in the Cretaceous period. The overprint of two-episodic tectonism processes caused several faults with high hydraulic conductivity. See the figures above for the field data.

3.2 Water sampling and methods

A field investigation was further conducted in the Xiayunling–Longmentai synclinorium hydrogeological unit based on the geologic, tectonic, and hydrogeologic backgrounds of the Fangshan area. Moreover, 30 representative water samples from the recharge, runoff, and discharge areas were collected, including 29 groundwater (Springs and Karst groundwater) sampled from the Wumishan aquifer (Jx*w*) and one surface water from Juma River, as shown in Figure 1B. Water samples were taken when pumping is stable to make sure the indicators like conductivity, and the redox potential are stable. Total dissolved solids (TDS), pH, and total hardness (TH) were measured *in situ* with YSI Professional Plus handheld multiparameter instrument which was calibrated with standard solutions. All samples were preserved at temperature less than 4°C in acid-washed

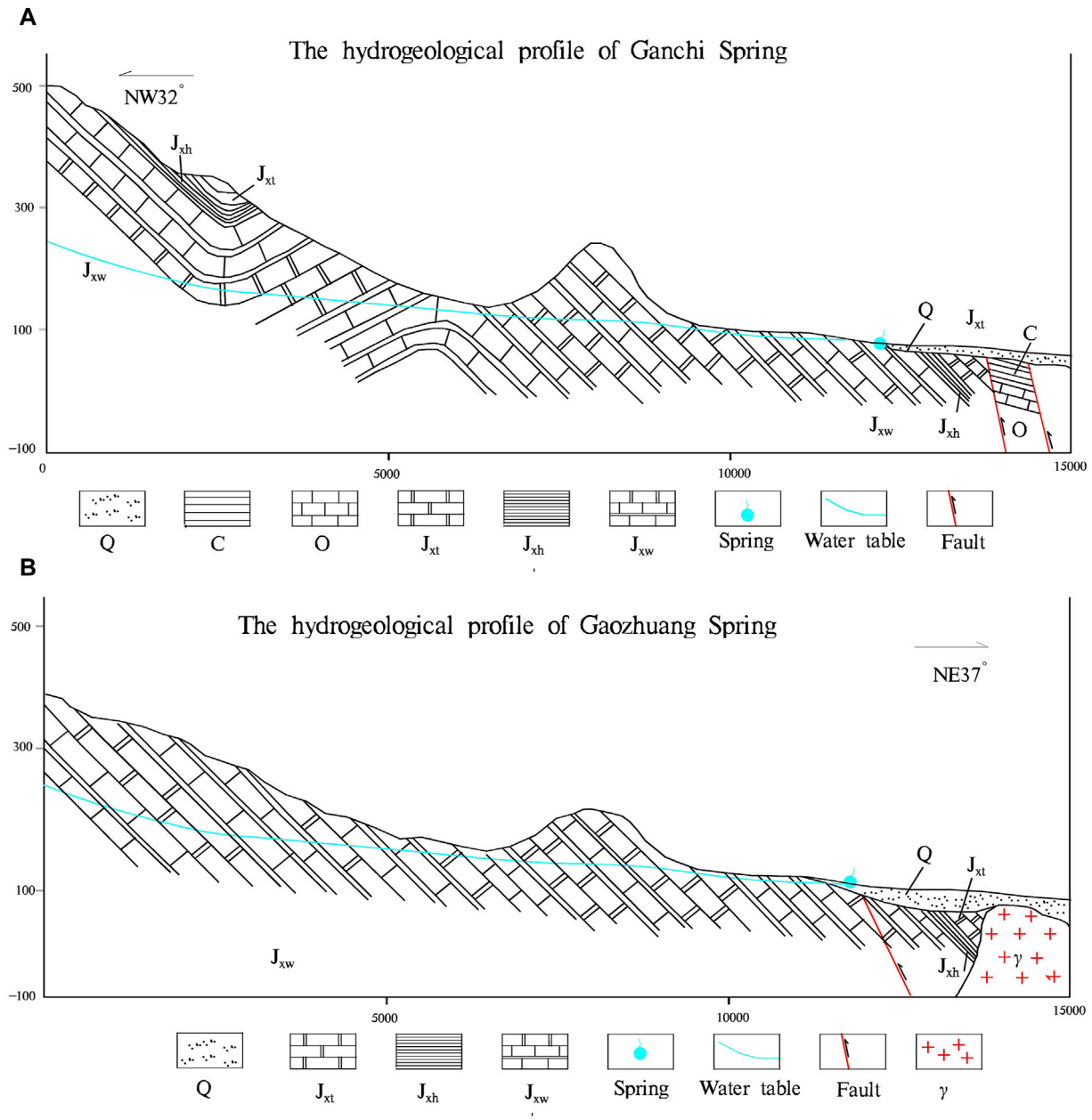

FIGURE 3
(A) profile of Gaozhuang springs **(B)**. Profile of Ganchi springs.

polyethylene bottles with watertight caps until analyzing processes as required by standard procedures.

Groundwater samples for hydrochemical analysis were filtered in the field using a 0.45 μm cellulose acetate filter membrane, and samples for cation analysis were acidified to pH < 2 with 6N HNO_3. The alkalinity of water samples was determined by titration with H_2SO_4 (0.22N) on the day of sample collection. The hydrochemical composition was analyzed for cations (Na^+, K^+, Mg^{2+}, Ca^{2+}, and Sr^{2+}) by inductively coupled plasma (ICP). The ion chromatography determined Cl^-, SO_4^{2-}, NO_3^-, and F^- concentrations. All the water samples were analyzed at the Key Laboratory of Shale Gas and Geoengineering, Institute of Geology and Geophysics, Chinese Academy of Science (CAS).

4 Results

4.1 Groundwater chemical condition

As shown in Table 1, the pH was between 7.03 and 7.79, being weakly alkaline with a small coefficient of variation. The coefficients of variation of $Cl^-$and $NO_3^-$are 171% and 101%, indicating that the degree of variation in space is very large. Mg^{2+}, $HCO_3^-$and F^-ions are 22%, 18% and 27%, respectively, which is lower than the coefficient of variation of the remaining ions, indicating that the spatial divergence of these ions is weak. Anion coefficient of variation from large to small order $Cl^- > NO_3^- > SO_4^{2-} > F^- > HCO_3^-$, $Cl^-$and NO_3^-spatial variation is strong. The maximum values of $Cl^-$and

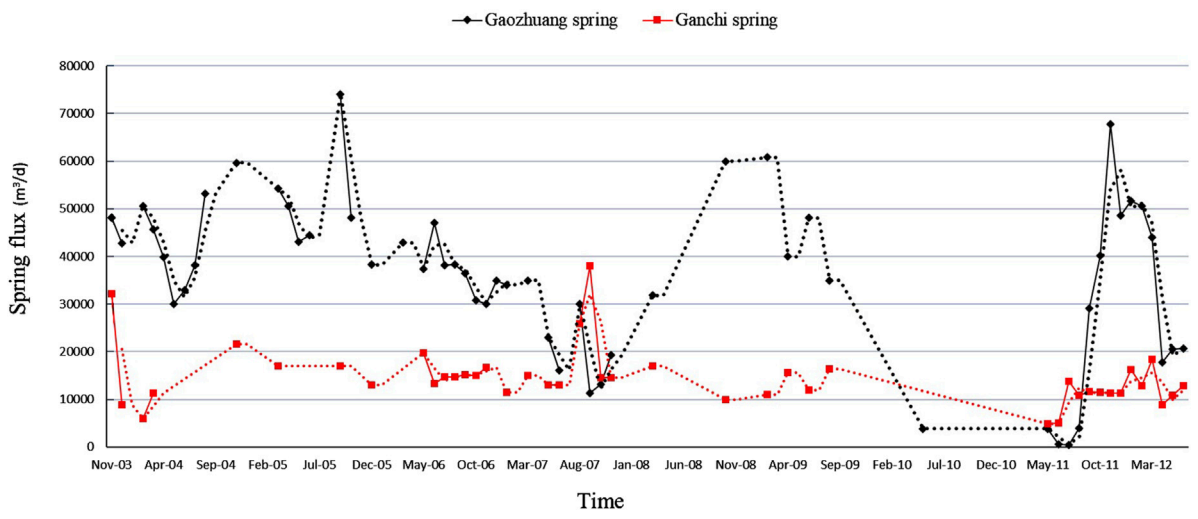

FIGURE 4
Fluctuation curve of Gaozhuang and Ganchi springs.

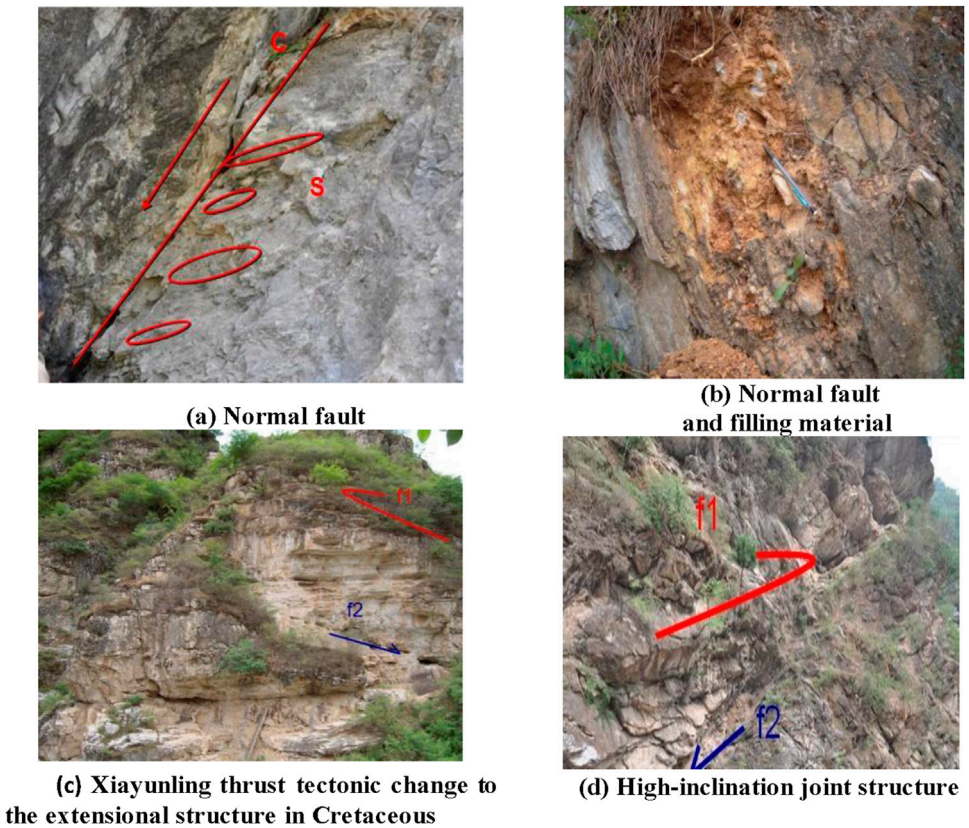

FIGURE 5
Geological bodies formed by overprint of two-episodic tectonism processes (f1 is thrust nappe structure and the f2 is extension structure). **(A)** Normal fault **(B)** Normal fault and filling material **(C)** Xiayunling thrust tectonic change to the extensional structure in Cretaceous **(D)** High-inclination joint structure.

NO_3^- in the samples are 78.65 mg/L and 30.36 mg/L, respectively, and appeared in Huangyuansi Village (ZF012), where the TDS value was also the maximum, which are most likely derived from the effects of human.

4.2 Groundwater chemical type

Water samples were taken from various sources, including surface water, springs, and karst groundwater. According to the

TABLE 1 Groundwater sample test results.

	Min	Max	Average	Standard deviation	Coefficient of variation/%
pH	7.03	7.79	7.44	0.17	2.24
TH	139.80	462.90	227.50	64.40	28.30
TDS (mg/L)	186.60	630.00	277.20	87.70	31.63
Ca^{2+}/(mg/L)	29.60	120.00	50.00	17.92	35.85
Mg^{2+}/(mg/L)	15.70	39.10	24.60	5.58	22.66
$Na^{+}+K^{+}$/(mg/L)	2.41	34.95	7.28	6.20	85.18
Sr^{2+}/(μg/L)	31.50	181.00	71.63	41.41	57.80
SO_4^{2-}/(mg/L)	9.75	102.51	43.92	26.81	61.03
HCO_3^{-}/(mg/L)	156.20	348.00	221.85	40.58	18.29
Cl^{-}/(mg/L)	4.44	78.65	11.88	14.00	117.85
NO_3^{-}/(mg/L)	0.59	30.36	7.51	7.64	101.72
F^{-}/(mg/L)	0.09	0.31	0.20	0.05	26.95

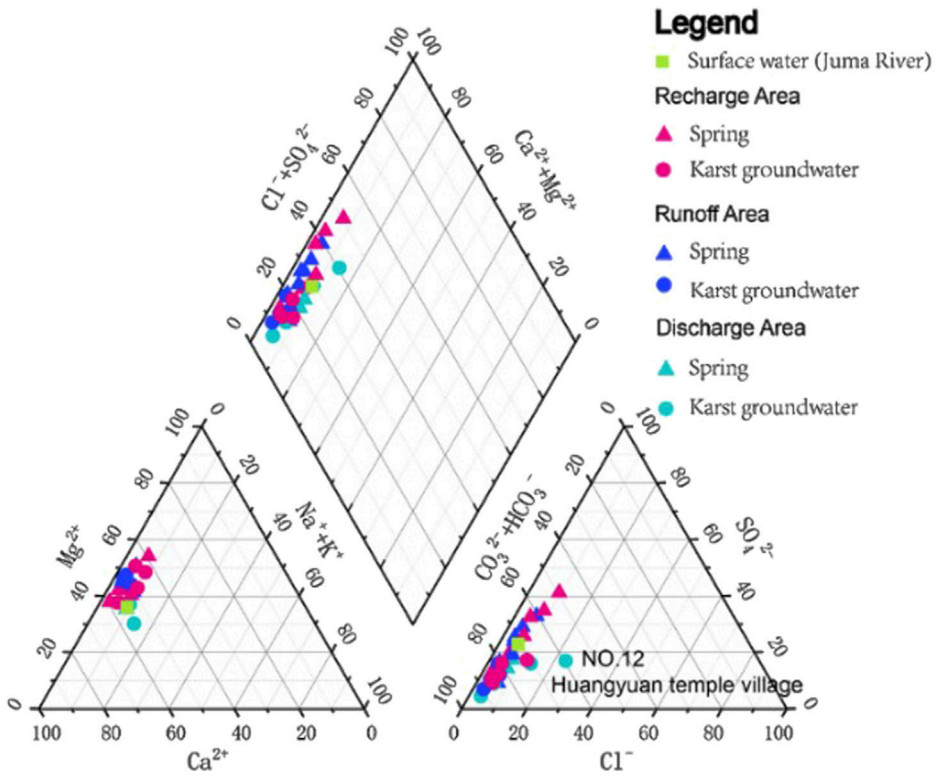

FIGURE 6
Piper trilinear plot for the chemical composition of water samples in the study area.

sampling location in the study area, the data were divided into three groups recharge, runoff, and discharge areas. Groundwater samples were plotted onto Piper trilinear graph based on hydrochemical data (Figure 6). The cation is dominated by Ca^{2+} and Mg^{2+}, while the anion is predominated by HCO_3^{-} and SO_4^{2}. The percentage of milligram equivalent for SO_4^{2-} in springs is larger than that in karst groundwater, while that of HCO_3^{-} shows the opposite. Hydrogeochemical types based on Shoka Lev classification methods are divided into HCO_3-Ca·Mg, HCO_3·SO_4-Ca·Mg, and HCO_3-Mg·Ca, which account for approximately 68%, 19%, and 13%, respectively. The distribution of cations and anions is relatively concentrated, which indicates the consistency with the hydrochemical type (HCO_3-Ca·Mg) in the study area.

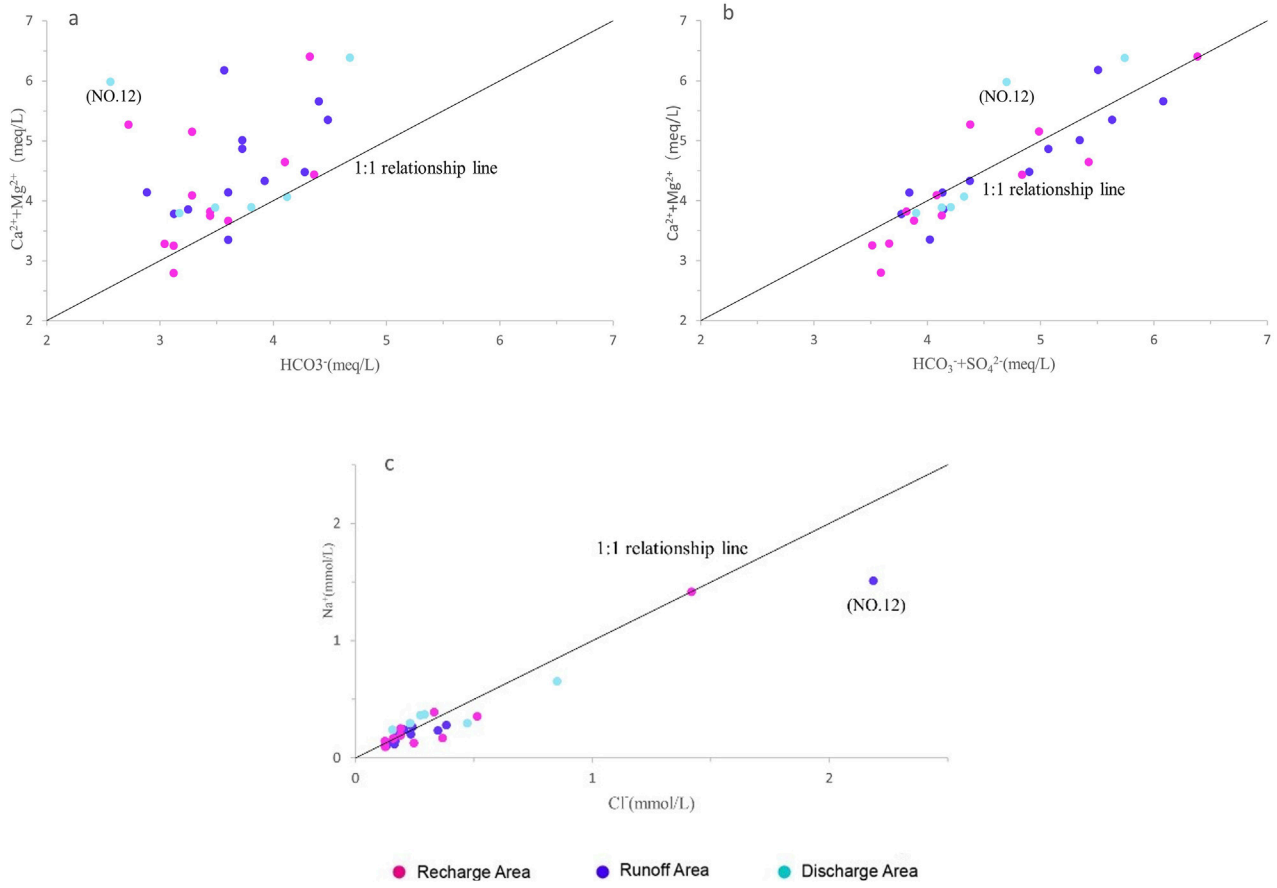

FIGURE 7
Diagram of the co-variation between main chemical components **(A)** $Ca^{2+}+Mg^{2+}$ vs. HCO_3^-; **(B)** $Ca^{2+}+Mg^{2+}$ vs. HCO_3^- + SO_4^{2-}; **(C)** Na^{2+} vs. Cl^-.

4.3 Main relations

According to the karst Equations 1–3 below. The main ion composition and proportion property may be used to analyze the origin of chemical composition and formation process:

$$(a)\ CaCO_3 + H_2O + CO_2(g) = Ca^{2+} + 2HCO_3^- \quad (1)$$

$$(b)\ CaMg(CO_3)_2 + 2CO_2(g) + 2H_2O = Ca^{2+} + Mg^{2+} + 4HCO_3^- \quad (2)$$

$$(c)\ CaCO_3 + CaMg(CO_3)_2 + 3CO_2 + 3H_2O = 2Ca^{2+} + Mg^{2+} + 6HCO_3^- \quad (3)$$

The main chemical components of groundwater are predominated by Ca^{2+}, Mg^{2+}, HCO_3^-, and SO_4^{2-} in the area under consideration. The origin of these components is closely related to the dissolution and precipitation of the main minerals in the aquifer, including calcium carbonate, dolomite, and gypsum. In natural karst groundwater systems, the equivalent concentration ratio of $[Ca^{2+}+Mg^{2+}]/[HCO_3^-]$ is 1:1 theoretically (Pu et al., 2014). Most of the groundwater samples in the study area are located to the left of the 1:1 line for $[Ca^{2+}+Mg^{2+}]/[HCO_3^-]$ in Figure 7A.

The concentration of Ca^{2+} and Mg^{2+} largely exceeded the equivalent concentration of HCO_3^-, and additional anions are needed to account for the excess concentrations of Ca^{2+} and Mg^{2+} relative to HCO_3^-. The increase in TDS accompanies an increase in Ca^{2+} and Mg^{2+}. This condition shows that the erosion of carbonate minerals is the main factor influencing karst groundwater chemical composition, thereby leading to the enrichment of Ca^{2+} and Mg^{2+} and the increase in total hardness and TDS content. Furthermore, a correlation is found between the concentrations of Ca^{2+}, SO_4^{2-}, and TDS. This correlation implies that additional gypsum minerals can be dissolved along with the groundwater flow direction, which can then release additional Ca^{2+} into groundwater. When SO_4^{2-} is added to the denominator of $[Ca^{2+}+Mg^{2+}]/[HCO_3^-]$, the samples are on the verge of the 1:1 line in Figure 7B. This phenomenon shows that SO_4^{2-} affects the ion electrovalent balance in these groundwater samples, and Ca^{2+} are not only mainly obtained from carbonate but also from gypsum dissolution in karst groundwater (Yidana and Yidana, 2010; Yu et al., 2012).

In addition, a significant correlation is observed between Cl^- and Na^+ (reaching up to 0.96). Therefore, Na^+ and Cl^- are derived from similar sources. The clastic rocks and other halite minerals within the study area are dissolved, thus enabling groundwater to generate Na^+ and Cl^- in the dissolution process. Groundwater samples (NO.12) in Huangyuan temple village is an abnormal point whose concentration of Cl^- is as high as 78.65 mg/L and deviates from the 1:1 relationship line (Figure 7C). Anthropic origin was a possible response to extreme values.

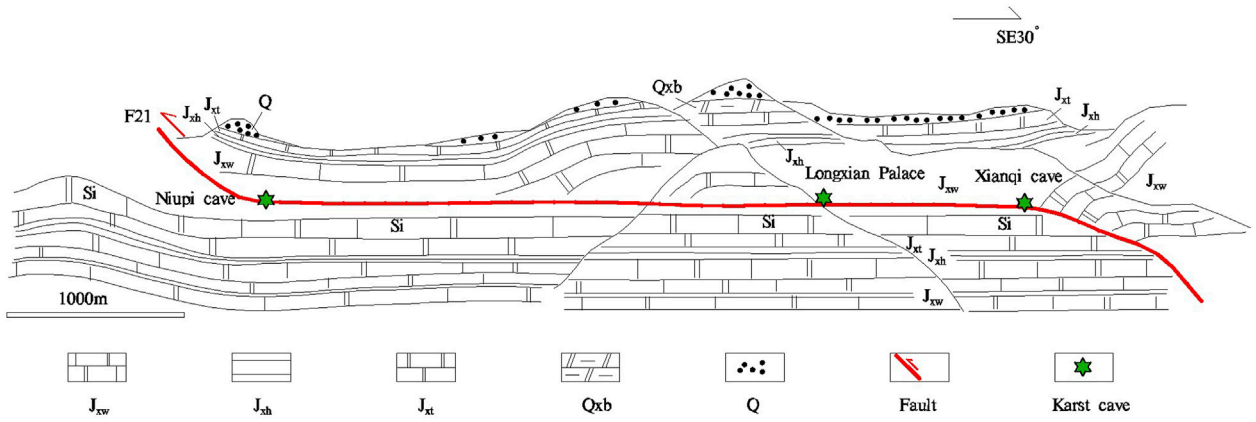

FIGURE 8
Patterns of cave distribution.

FIGURE 9
Interlayer fissure in horizontal caverns.

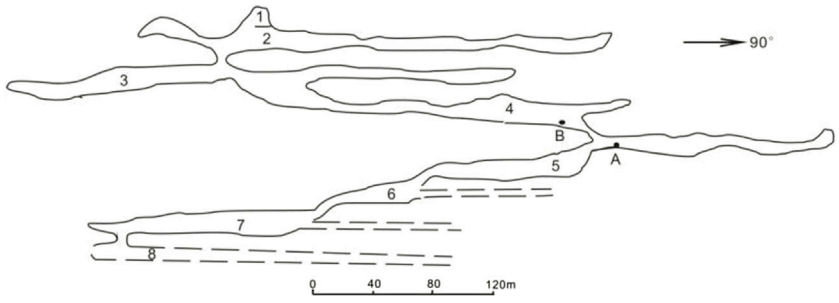

FIGURE 10
Multiple uplift erosion karst cave models.

4.4 TDS distribution

In this area, the mean value of TDS was 282.9 mg/L, and the mineralization degree was low. The spatial distribution of TDS is shown in Figure 12A. In the recharge area (the northern part of the exposed limestone area, which is near the southern plain), karst groundwater was recharged from atmospheric precipitation, and the TDS of water samples is low (average value of 261.6 mg/L). TDS gradually increases along a circulation path, which is relatively high in the hilly area (Nos. 13 and 15; 403 and 323 mg/L, respectively). However, groundwater near Xiayunling-Dayugou (F21) and other fault-concentrated areas has a low concentration of TDS (less than

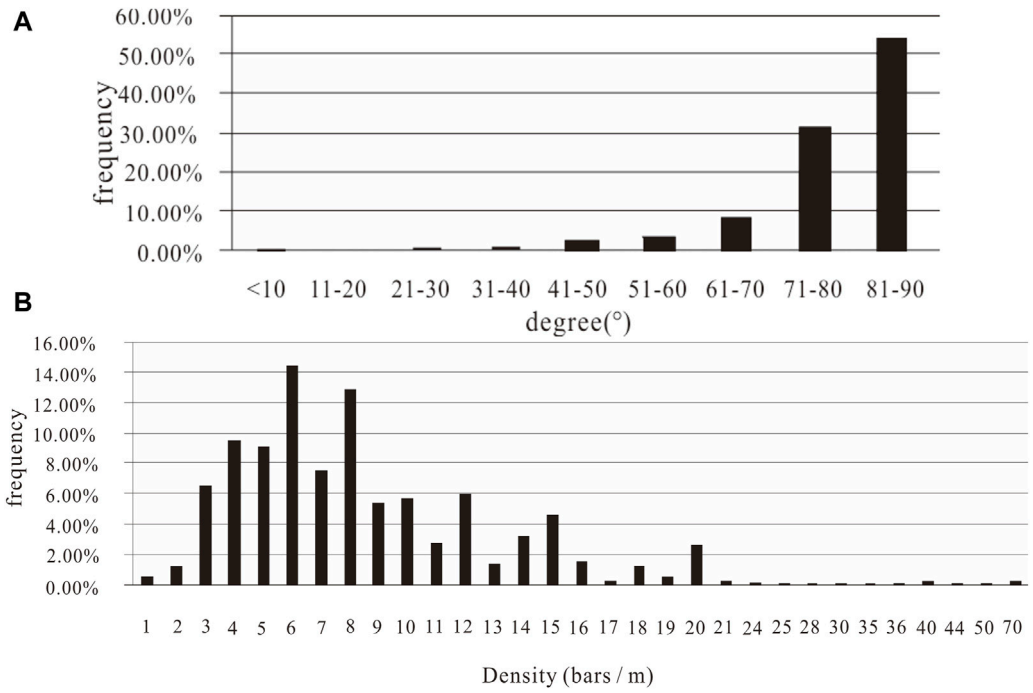

FIGURE 11
(A) Statistical analysis of joint degree of fractures **(B)** Statistical analysis of joint density of fracture.

247 mg/L). TDS with high value is mainly distributed in the discharge area; for example, the TDS of Huangyuan Temple is as high as 630 mg/L. The TDS considerably increases along the groundwater flow from northwest to southeast as a whole.

5 Discussion

5.1 Cave distribution regulation controlled by structure and hydrodynamic conditions

Numerous joint structures have been developed in the multistage and multigeneration structural deformation in the study area. The dominant fracture azimuth of NEE and NNW is frequent in multiple groups of fissures. The cracks in other directions are also biased by NE and NW. Comparing the characteristics of joints in the two large-scale fractures, joint distribution direction developed along two dominant fracture directions, namely NNW and NE. The north-south joint controls the extending direction of the cave, and the east-west joint restricts the lateral development.

Lots of the large caverns in this area, such as Xianqi cave, Longxian Palace and Niupi cave in Xiayunling thrust fault (F7), and Yunshui cave in Huangshandian thrust fault zone (F6), are developed in or near the fault zone in Figure 1. These caves are developed on the Xiayunling thrust fault and are consistent with the direction of the Xiayunling fold-back thrust nappe structure, and the extension direction of fracture affects the development direction of karst, as shown in Figure 8.

Lots of interlayer karst caves develop along the contact zone or unconformity between solute and non-solute rocks (Figure 9). The bedding planes are of considerable importance to the cave development in this area. Especially in the widely distributed Jxw siliceous dolomite, the occurrence of the strata is gentle. Moreover, thin layers with sericite schist and siliceous strip are found in the rock mass, which often forms a weak water-isolation layer and becomes the base of the cave development. The development of the interlayer karst caves shows that there is a huge degree difference of water-rock interaction, which completely depends on the mobility of the water and the solubility of the rock.

A series of large karst caves have been found in the mountainous area of Ordovician limestone outcrop in Fangshan District. For example, the Yunshui cave is developed on the Huangshandian thrust fault zone, and a series of high-angle normal faults with north-south strike (F1-F6) are formed, which control the spatial position of Yunshui cave in the karst structure, as shown in the below Figure 10.

Regularly, multi-layer cave is related to vertical hydrodynamic conditions which a strong hydrodynamic response to the of vertical crustal movement. Groundwater is mainly vertical movement in dry season while keeps horizontal movement in rainy season. With each rise of the earth's crust, the decline of the local erosion datum and the appearance of the crack point, the spatial form of the cave decreases step by step, forming the model of multi-layer karst cave.

5.2 Indicating from TDS and Sr

Total dissolved solids (TDS) are a major indicator of each component concentration in groundwater. In the study area, the geological structure initially affects TDS distribution through a series

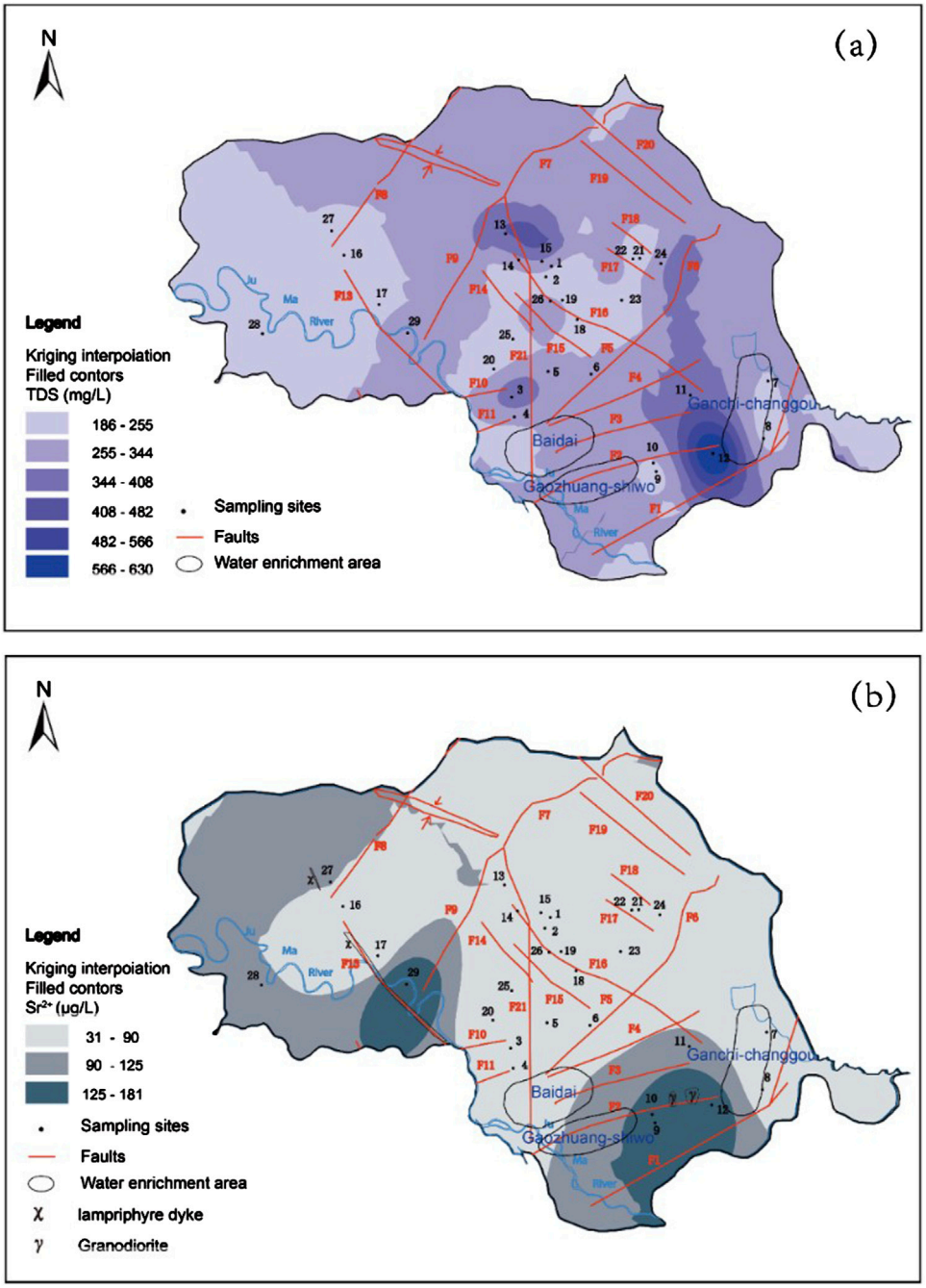

FIGURE 12
(A) TDS distribution of groundwater in the hydrogeological unit; **(B)** Strontium distribution of groundwater in the hydrogeological unit.

of NW and NE-trending faults and a topography that is lower in the east and south than that in the west and north in the areas. For the NW-trending faults, groundwater follows its direction and flows from northwest to southeast. By contrast, for the NE-trending faults, groundwater migrates from northwest to southeast accompanying transverse fractures. The two groups of faults form a grid structure, which creates a uniform aquifer for groundwater and provides a favorable way for large-scale deep runoff.

On the one hand, the overall yield of the joints has obvious regional structural fracture characteristics, and shows the conjugation characteristics of the structural joints. In most areas, the development direction is relatively concentrated, the dominant joints are prominent, and the development direction of a few areas is scattered, indicating that its joint formation is affected by multi-stage tectonic stress. A large number of tectonic cracks have been developed in multiple phases and multiple tectonic deformations, mainly for high-angle joints, high development density and large depth. It shows that the joints with dip angles between 81° and 90° in the field account for 53.79% of the total joints. Joints between 71° and 80° account for 31.29% and between 61° and 70° joints account

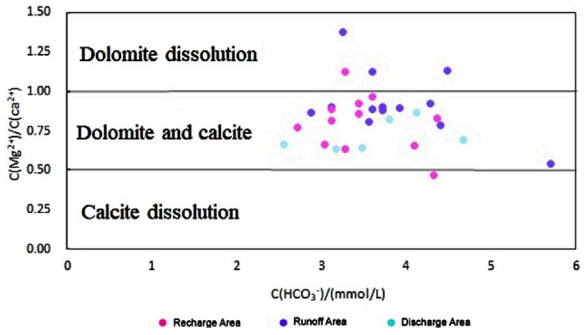

FIGURE 13
Plots of HCO_3^- against Mg^{2+}/Ca^{2+} in karst groundwater in Zhangfang.

for 7.95% of the total number of joints. Low and medium angle joints do not exceed 7% of the total number of joints. Such faults are straight over long distances and the fault plane is nearly vertical, as showed in Figure 11A. The joint density is large in the study area and ranges from 1/m to 70/m. It can be seen from the diagram that the density of joints is important in the range of 3/m to 15/m. The proportion of 6/m was the largest (14.44%), followed by 8 joints/m density, as showed in Figure 11B. The vertical infiltration speed is fast, and the water alternation is fast, providing the transport channel of atmospheric precipitation and surface water infiltration.

On the other hand, the junction parts of different azimuth faults and the junction parts of main fracture and branch fracture, the development of tension cracks and torsion cracks are conducive to the movement of groundwater, which is not only a water storage space, but also a catchment corridor, often forming a fault water-rich belt. Especially in the soluble rocks, the broken rock is badly broken, and the width of the influence zone is large, which is a good place for groundwater enrichment.

Strontium is an easy migration element in water, and its content is substantially low in atmospheric precipitation. The enrichment of Sr^{2+} in groundwater is affected by the supply source, aqueous medium, and the intensity of water–rock interaction (Klaus, Hansen, and Buapeng, 2007; Shand et al., 2009). Sr concentrations vary from 31.5 μg/L to 181 μg/L of groundwater in the study area (Figure 12B). Lamprophyre dyke (χ), which is along the southeast direction, is exposed to the western of Fangshan. The magmatic rock (γ) mass exposed to Shimen village, which is north of Gaozhuang spring, has a distribution area of around 1 km^2, and its lithology is granodiorite. The groundwater collected neighboring intrusive rocks (including lamprophyre (χ) and magmatic rock (γ)), which have higher Sr concentrations (Nos. 09, 10, 11, and 29 are 150, 139, 161, and 181 μg/L, respectively) compared with those from other flow fields with less than 100 μg/L. This finding is attributed to water–rock interaction between groundwater and intrusive rocks containing high Sr contents (Cai et al., 2005; Tao et al., 2006).

5.3 Geochemical process and hydrochemical evolution in the flow field

Numerous geochemical processes control the evolution of groundwater. This evolution is predominantly controlled by evaporation–precipitation, water–rock interaction, and atmospheric precipitation in the study area.

The ratio of magnesium–calcium ions in karst groundwater is mainly controlled by the ratio of calcite to dolomite in strata (Pu

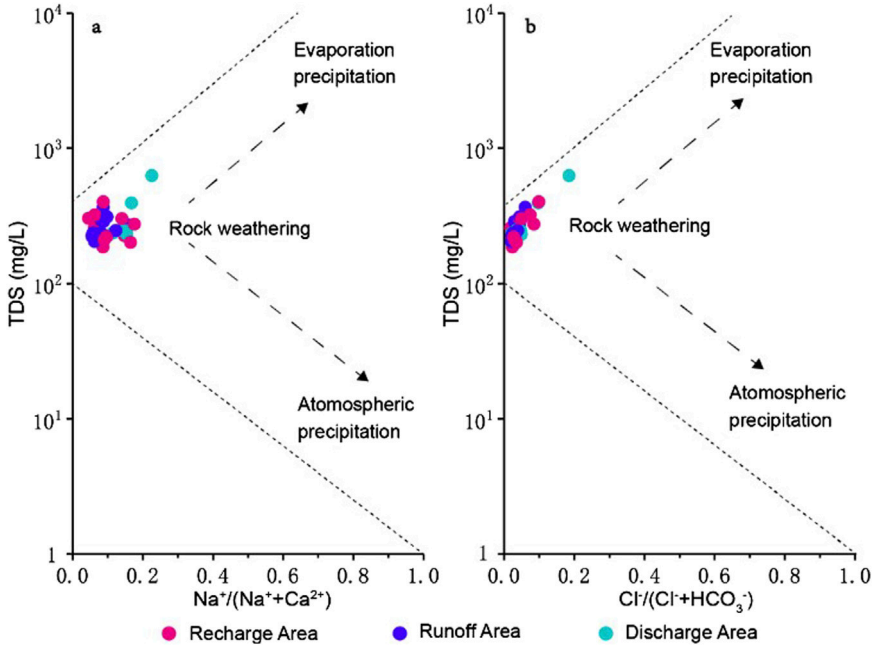

FIGURE 14
Hydrogeologic Gibbs diagrams for groundwater samples **(A)** TDS vs. $Na^+/(Na^+ + Ca^{2+})$ weight ratio; **(B)** TDS vs. $Cl^-/(Cl^- + HCO_3^-)$ weight ration.

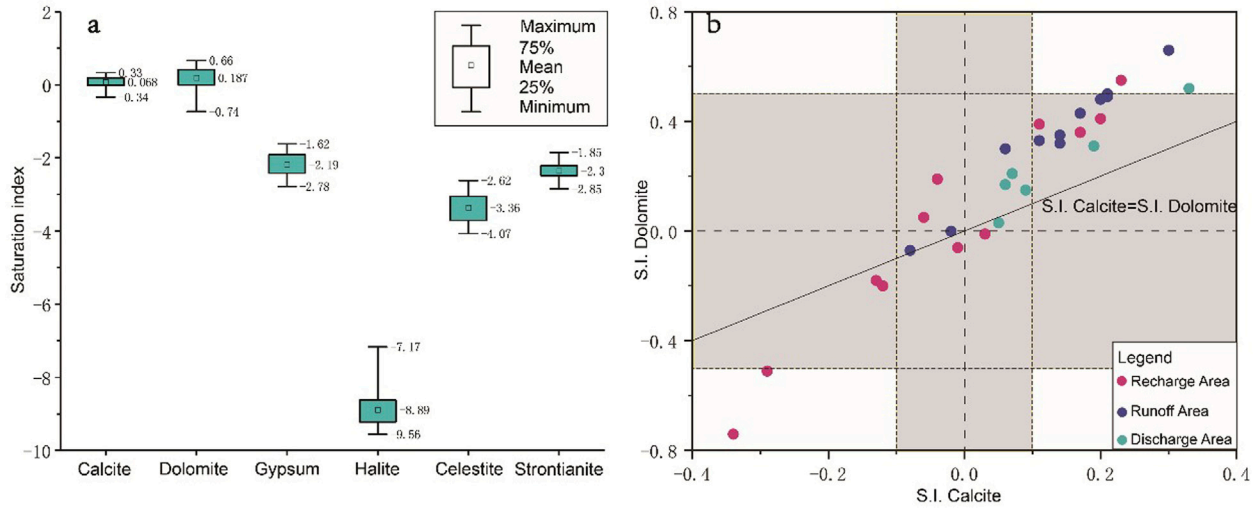

FIGURE 15
(A) Box-plot graph for saturation indexes for groundwater in the study area. **(B)** $SI_{Dolomite}$ vs. $SI_{calcite}$ for the groundwater samples. (Distribution of uncertainty (shaded areas) of ±0.5 and ±0.1 units in $SI_{Dolomite}$ and $SI_{calcite}$, respectively, can indicate equilibrium or near-saturation considering these minerals).

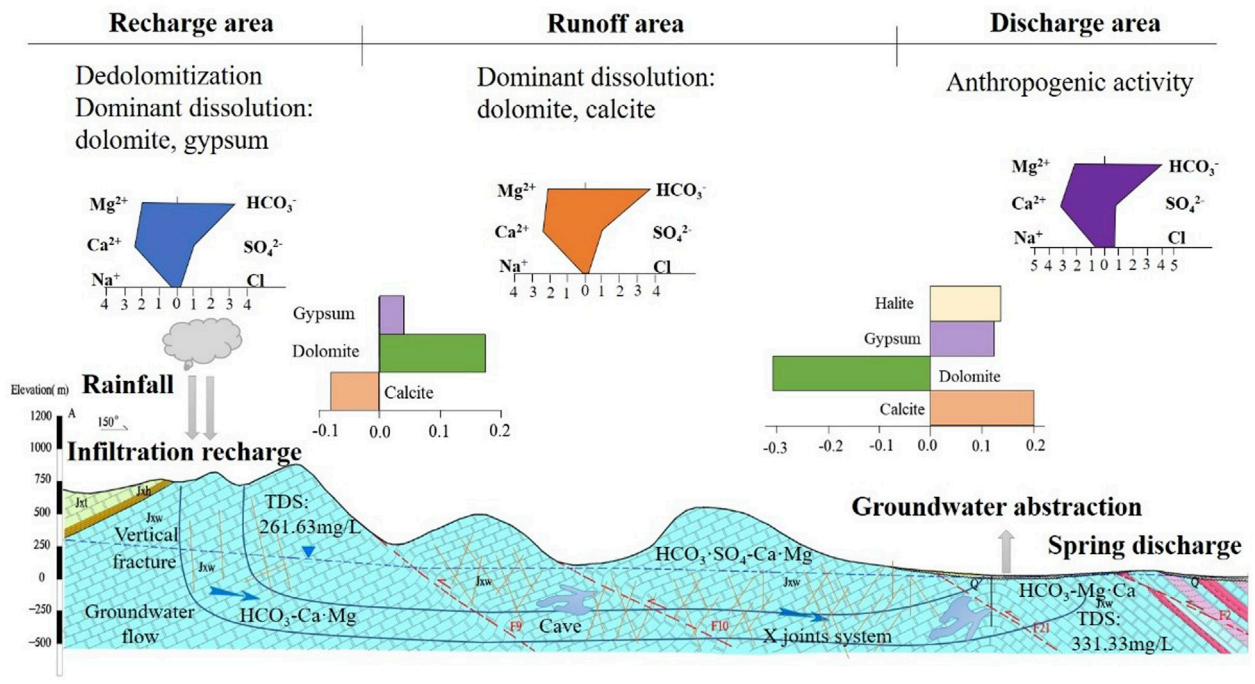

FIGURE 16
A hydrogeological conceptual model for hydrochemical process and evolution in the study area from northwest to southeast.

et al., 2010). When calcite and dolomite are dissolved in equilibrium $c(Mg^{2+})/c(Ca^{2+}) = 0.5$, only dolomite reaches the equilibrium of dissolution, that is, $c(Mg^{2+})/c(Ca^{2+}) = 1$. When only calcite reaches the equilibrium of dissolution, no magnesium ions are dissolved, that is, $c(Mg^{2+})/c(Ca^{2+}) = 0$. Figure 13 shows that the dissolved components of water samples in the study area mainly comprise calcite and dolomite, and some of these components are mainly controlled by dolomite dissolution. This finding is consistent with the extensive development of dolomite in the study area.

The Gibbs diagram was initially used to represent the influence mechanism of surface water chemical composition (Rose, 2007). In recent years, many scholars have also used this method to distinguish the primary processes controlling the hydrogeochemical characteristics of groundwater (Kumar et al., 2016; Nazzal et al., 2014). The Gibbs

diagram contains three zones, including rock weathering, evaporation–precipitation, and atmospheric precipitation (Gibbs, 1970).

All the ion compositions of karst groundwater in this area in the Gibbs model converged in the rock weathering zone, as shown in Figure 14. Such convergence means that the ions of karst groundwater in the study area mainly come from rock weathering. In addition, some water samples in the middle and east tend to the control end of evaporative crystallization.

The saturation index (SI) is beneficial to evaluate the equilibrium between water and minerals and illustrate the water–rock interaction in the karst aquifer system (Moore et al., 2010). The saturation state is calculated through a comparison of the activities in water samples (ion activity product) and those at equilibrium (solubility product). The comparison results are beneficial in the assessment of the evolution stage of a groundwater sample and the identification of the controlling geochemical reactions (Appelo and Postma et al., 2005). PHREEQC (Parkhurst and Appelo, 2011) was used to assess the saturation indexes for the groundwater samples. The results displayed by the box plot (Figure 15A) reveal that the values of $SI_{calcite}$ and $SI_{dolomite}$ are close to zero, while those of others (SI_{gypsum}, SI_{halite}, $SI_{celesite}$, and $SI_{strotianite}$) are negative. Moreover, the values of SI_{halite} were far below zero. This finding confirms that most groundwater samples are oversaturated or close to equilibrium considering calcite and dolomite. Meanwhile, gypsum, halite, celestite, and strontianite did not reach equilibrium and can still be dissolved into groundwater. This finding indicates the presence of calcite and dolomite minerals in the aquifer system, which controls the chemical composition of the groundwater. Additionally, gypsum, halite, celesite, and strontianite mineral sources are insufficient in the study area, thereby resulting in limited interactions between groundwater and these minerals. Groundwater samples are typically closer to the shaded zone with dolomite than with calcite (Figure 15).

6 Groundwater system conceptual model

A conceptual model of groundwater flow and geochemical evolution was applied based on the aforementioned fracture distribution and hydrogeochemical to investigate the hydrogeological conditions in the study area (Figure 16).

From recharge to runoff to discharge areas, hydrogeochemical types generally have almost no change (HCO_3-Ca·Mg), but ionic composition regularly varies. The milligram equivalent for Ca^{2+} (1.95→2.09), Na^{+}+K^{+} (15.20→16.07), Cl^{-} (0.27→0.68), and HCO_3^{-} (3.34→4.16) gradually increases, while that of SO_4^{2-} (0.98→0.78) generally decreased along the flow path. For the cation Mg^{2+}, the concentration first rises from 23.37 mg/L in the recharge area to 25.72 mg/L in the runoff area and then reduces to 25.03 mg/L in the discharge area.

In the recharge area, local atmospheric precipitation is the dominant recharge of groundwater. Many vertical or high inclination joints lead to direct infiltration of rainwater, which has good conductivity but low poor water storage. Groundwater quality is generally good, and the average value of TDS is 261.63 mg/L. From mountainous areas in the northwest to the plain in the southeast, the fissures developed from weak to strong overall.

In the runoff area, the multiple groups of fractures with high density and good permeability form a crisscross network of dissolution fractures, which becomes a channel for groundwater infiltration and runoff. Particularly, the fissures are increasingly developed in the fracture contact zones along the Xiayunling thrust fault (F7) and Dayugou fault (F21) from north to south. Numerous caves occur around this area. These regional faults formed not only the runoff channel but also constituted the storage space of regional groundwater–rock interaction. TDS increased to 300–400 mg/L along the flow direction. Most groundwater samples are typically supersaturated with calcite, thereby indicating that the reaction process between groundwater and calcite minerals also occurs from runoff to discharge area. Simultaneously, the concentration of SO_4^{2-} increases progressively possibly due to the dissolution of gypsum minerals. Meanwhile, the dedolomitization process exists in the groundwater, thus leading to an increase in the milligram equivalent of Mg^{2+} from runoff to the discharge area.

Along groundwater flow direction, water–rock interaction is a significant process during groundwater hydrogeochemical evolution. The mean value of TDS in the discharge area reached 630 mg/L, thereby indicating the TDS gradually increase with runoff distance along the karst water flow. Particularly in Huangyuan temple village (No. 12), extreme values of Cl^{-} and NO_3^{-} are found, suggesting the effect of anthropic origin. The increment of Ca^{2+} (15.06→16.07) resulted in a decrease in Mg^{2+} (2.14→2.09). Therefore, dolomite precipitation and gypsum, halite, and calcite are the dominant dissolutions of reactants. The water-resisting structures, such as the dike and rock mass, controlled the formation of Gaozhuang and Ganchi springs, but karst fissure aquifers developed in the deep part through the vertical profile. This finding indicates that the circulation depth of groundwater is deep, thus resulting in sufficient water–rock interaction, which promotes the development of deep karst. Meanwhile, the sulfate reduction in deep runoff resulted in the occurrence of desulfation. Consequently, the concentration of SO_4^{2-} progressively reduces along the groundwater direction.

7 Conclusion

The development and distribution of the karst fracture has considerable practical significance for the understanding of karst cave development and hydrochemical characteristic evolution in large-scale karst spring systems. Known as fissure-karst water-bearing system, erosion fissure is the most common karst form in groundwater system in North China, therefore, the main controlling factor of karst development is geological structure and groundwater flow field in the fissure-karst water system. In order to analyze the relationship of the chemical component evolution in karst fracture media with tectonic characteristic, this study systematically analyzed structure control on hydrochemical indicators for karst development perspective of the groundwater flow in Fangshan, Beijing, North China.

The structures in this area controlled not only groundwater flow direction from northwest to southeast but also the characteristic of hydrochemical in spatial distribution. Eventually, with the cooperation, they affect the karst development. The hydrogeochemical is mainly HCO_3-Ca·Mg and TDS increase from 261 mg/L to 630 mg/L along groundwater flow. All the ion compositions of karst groundwater in this area in the Gibbs model converged in the rock weathering zone, meaning that the ions of karst groundwater in the study area mainly come from rock weathering dominated by the interaction of water and carbonate minerals. From recharge to the discharge area, the increases

of Mg^{2+} mainly due to dedolomitization process and the desulfation results in sulfate reduction. The anthropogenic contribution in the discharge area cannot be ignored.

The high dip angle or vertical dips are benefit to infiltration directly. The overprint of two-episodic tectonism processes (thrusting nappe structure in Jurassic period and extensional structure in Cretaceous period) caused a series of NE-NW fold-back thrust nappe structures and a number of faults intersection areas composing the groundwater runoff channels and WRI space. Therefore, the direction of karst cave development and distribution is controlled by the development extension of faults. For example, the development direction of a serious of karst caves is consistent with the direction of the Xiayunling fold-back thrust nappe structure. Tectonic movement, especially the multi-stage tectonic activity, has an important impact on the development of caves, such as Shihua cave. The density of joints affects the degree of karst development. While, some structures do block water. High Sr concentrations are observed in the north intrusive rocks due to the effect of the intrusive structure.

The understanding of structures' influence is benefit to understanding groundwater distribution and geochemistry evolution in karst water system. Although the analysis is systematic and integrated, there are still many shortcomings in the current work. For example, the sampling of the two plates around the fault is subject to various restrictions, and there is not sufficient data. In the future work, we will increase the number of samples. Especially, sample collection on both sides of the fault also needs to be strengthened for a better comparative study. The concept of karst groundwater system could be used as an exemplar of a karst aquifer, which is of instructive significance and has practical value in other similar areas of North China. Our work can provide a basis for further formulating the planning of water exploitation and utilization and the target area of karst water exploration in lots of northern city.

Data availability statement

The original contributions presented in the study are included in the article/Supplementary Material, further inquiries can be directed to the corresponding author.

Author contributions

QX: Writing–original draft, Writing–review and editing. LB: Writing–review and editing. LK: Writing–review and editing, Conceptualization. CX: Writing–review and editing, Validation. YW: Data curation, Writing–review and editing.

Funding

The author(s) declare that financial support was received for the research, authorship, and/or publication of this article. This study is jointly supported by the National Natural Science Foundation of China (No. 42372298), National Key Research and Development Program of China (No. 2020YFC1807104), Fundamental Research Funds for the Central Universities and the Fundamental Research Funds for the Central Universities and Beijing Karst Water Resources Exploration and Evaluation Project (BJYRS-ZT-03).

Acknowledgments

We thank all the reviewers for their valuable comments and suggestions.

Conflict of interest

The authors declare that the research was conducted in the absence of any commercial or financial relationships that could be construed as a potential conflict of interest.

Publisher's note

Supplementary material

The Supplementary Material for this article can be found online at: https://www.frontiersin.org/articles/10.3389/fenvs.2024.1494730/full#supplementary-material

References

Andreo, B., Vías, J., Durán, J. J., Jiménez, P., López-Geta, J. A., and Carrasco, F. (2008). Methodology for groundwater recharge assessment in carbonate aquifers: application to pilot sites in southern Spain. *Hydrogeology J.* 16, 911–925. doi:10.1007/s10040-008-0274-5

Appelo, C. A. J., and Postma, D. (2005). *Geochemistry, groundwater and pollution* (2nd ed.) CRC Press. doi:10.1201/9781439833544

Benischke, R., Goldscheider, N., and Smart, C. (2007). Tracer techniques, In: Editors N. Goldscheider and D. Drew *Methods in Karst Hydrogeology* (London, United Kingdom: Taylor and Francis Group), 147–170.

Bi, W. (1986). *Characteristics and distribution of karst landform in Fangshan, Beijing*. Beijing: Journal of Beijing Teachers Academy (Natural Science Edition), 64–70. doi:10.19789/j.1004-9398.1986.01.012

Boucher, M., Girard, J.-F., Legchenko, A., Baltassat, J.-M., Dörfligerc, J.-M., and Chalikakis, K. (2006). *Using 2D inversion of magnetic resonance soundings to locate a water-filled karst conduit*, 330, 413–421.

Cai, J., Yan, G., Mou, B., Ren., K., Song., B., and Li, F. (2005). Zircon U-Pb age, Sr-Nd-Pb isotopic compositions and trace element of Fangshan complex in Beijing and their petrogenesis significance. *Acta Petrol. Sin.* 21, 776–788. doi:10.3969/j.issn.1000-0569.2005.03.017

Cao, Y., Wang, Q., Li, L., Ji, Y., and Zhang, Y. (2014). Discussion on characteristics of the karst cave in Beijing Fangshan District. *Urban Geol.* 9, 17–20. doi:10.3969/j.issn.1007-1903.2014.01.005

Cartwright, I., Weaver., T. R., Cendón., D. I., Fifield, L. K., Tweed., S. O., Petrides, B., et al. (2012). Constraining groundwater flow, residence times, inter-aquifer mixing, and aquifer

properties using environmental isotopes in the southeast Murray Basin, Australia. *Appl. Geochem.* 27, 1698–1709. doi:10.1016/j.apgeochem.2012.02.006

Chu, H. B., Wei, J. H., Wang, R., and Xin, B. D. (2017). Characterizing the interaction of groundwater and surface water in the karst aquifer of Fangshan, Beijing (China). *Hydrogeology J.* 25, 575–588. doi:10.1007/s10040-016-1507-7

Dong, Y., Ju, Y. W., Zhang, Y. X., Rui, X. P., Bu, H., and Guo, G. X. (2014). *Characteristics of joints in karst area and their influence on karstification in Zhangfang in Fangshan region of Beijing. Journal of University of Chinese Academy of Sciences*, 31 (6), 83–790. doi:10.7523/j.issn.2095-6134.2014.06.009

Dreybrodt, W., Gabrovsek, F., and Romanov, D. (2005). *Processes of speleogenesis: a modeling approach*. Postojna, Slovenia: Karst Research Institute. Exploration and evaluation of karst groundwater in Fangshan.

Florea, L. J. (2015). Carbon flux and landscape evolution in epigenic karst aquifers modeled from geochemical mass balance. *Earth Surf. Process. and Landforms* 40, 1072–1087. doi:10.1002/esp.3709

Ford, D., and Williams, P. (2007). *Karst hydrogeology and geomorphology*. London: Wiley, 562.

Gibbs, R. J. (1970). Mechanisms controlling world water chemistry. *Science* 170, 1088–1090. doi:10.1126/science.170.3962.1088

Gil-Marquez, J. M., Barbera, J. A., Andreo, B., and Mudarra, M. (2017). Hydrological and geochemical processes constraining groundwater salinity in wetland areas related to evaporitic (karst) systems. A case study from Southern Spain. *J. Hydrology* 544, 538–554. doi:10.1016/j.jhydrol.2016.11.062

Gil-Márqueza, J. M., Sültenfußb, J., Andreoa, B., and Mudarraa, M. (2020) Groundwater dating tools (3H, 3He, 4He, CFC-12, SF6) coupled with hydrochemistry to evaluate the hydrogeological functioning of complex evaporite-karst settings, *J. Hydrology*, 580. 124263. doi:10.1016/j.jhydrol.2019.124263

Guo, G. X., Liu, W., Xin, B. D., Li, Y., and Shen, Y. Y. (2011). Current situations and discussions on karst groundwater resources exploration in Beijing. *South-to-North Water Divers. Water Sci. and Technol.* 9, 33–36+45. doi:10.3724/SP.J.1201.2011.02033

Illman, W. A., and Neuman, S. P. (2001). Type curve interpretation of a cross-hole pneumatic injection test in unsaturated fractured tuff. *Water Resour. Res.* 37 (3), 583–603. doi:10.1029/2000wr900273

Klaus, J. S., Hansen, B. T., and Buapeng, S. (2007). $^{87}Sr/^{86}Sr$ ratio: a natural tracer to monitor groundwater flow paths during artificial recharge in the Bangkok area, Thailand. *Hydrogeology J.* 15, 745–758. doi:10.1007/s10040-007-0175-z

Kollarits, S., Veselic, M., Kuschnig, G., Pavicic, A., Soccorso, C., and Aurighi, M. (2006). Decision-support systems for groundwater protection: innovative tools for resource management. *Environ. Geol.* 49, 840–848. doi:10.1007/s00254-006-0179-3

Kumar, M., Herbert, R., Jha, P. K., Deka, J. P., Rao, M. S., Ramanathan, A. L., et al. (2016). Understanding the seasonal dynamics of the groundwater hydrogeochemistry in national capital territory (NCT) of India through geochemical modelling. *Aquat. Geochem.* 22, 211–224. doi:10.1007/s10498-016-9289-z

Laskow, M., Gendler, M., I. Goldberg, M., Gvirtzman, H., and Frumkin, A. (2011). *Deep confined karst detection, analysis and paleo-hydrology reconstruction a basin-wide scale using new geophysical interpretation of borehole logs*, 406, 158–169.

Ledesma-Ruiz, R., Pasten-Zapata, E., Parra, R., Harter, T., and Mahlknecht, J. (2015). Investigation of the geochemical evolution of groundwater under agricultural land: a case study in northeastern Mexico. *J. Hydrology* 521, 410–423. doi:10.1016/j.jhydrol.2014.12.026

Li, S. J., (2012). A study of the characteristics and regulation-storage capacity of the Zhangfang karst-groundwater reservoir in beijing. A Dissertation Submitted to China University of Geoscience for Doctoral Degree.

Lv, J., Lu, Y., Zheng, G., and Zheng, M. (2010). Formation of karst cave system and its relationship with neotectonic movement in Beijing Western Hills, Beijing, China. *Geol. Bull. China* 29, 502–509. doi:10.3969/j.issn.1671-2552.2010.04.003

Lv, J. B., Li, T. Y., and Sun, Y. H. (1999). Karst geology of the Shi hua cave, Beijing. *Regional Geol. China* 18 (4), 373–378. (in Chinese with English abstract). doi:10.3969/j.issn.1671-2552.199

Marques, J. M., Graça, H., Eggenkamp, H. G. M., Neves, O., Carreira, P. M., Matias, M. J., et al. (2013). Isotopic and hydrochemical data as indicators of recharge areas, flow paths and water–rock interaction in the Caldas da Rainha-Quinta das Janelas thermomineral carbonate rock aquifer (Central Portugal). *J. Hydrology* 476, 302–313. doi:10.1016/j.jhydrol.2012.10.047

Mohamed, G., and Ahmed, S. (2017). Hydrogeochemical evaluation of fractured Limestone aquifer by applying a geochemical model in eastern Nile Valley, Egypt. *Environ. Earth Sci.* 76, 641. doi:10.1007/s12665-017-6974-1

Moore, P. J., Martin, J. B., Screaton, E. J., and Neuhoff, P. S. (2010). Conduit enlargement in an eogenetic karst aquifer. *J. Hydrology* 393, 143–155. doi:10.1016/j.jhydrol.2010.08.008

Nativ, R., Adar, E. M., and Becker, A. (1999). Designing a monitoring network for contaminated ground water in fractured chalk. *Ground Water* 37 (1), 38–47. doi:10.1111/j.1745-6584.1999.tb00956.x

Nazzal, Y., Ahmed, I., Al-Arifi, N. S. N., Ghrefat, H., Zaidi, F. K., El-Waheidi, M. M., et al. (2014). A pragmatic approach to study the groundwater quality suitability for domestic and agricultural usage, Saq aquifer, northwest of Saudi Arabia. *Environ. Monit. Assess.* 186, 4655–4667. doi:10.1007/s10661-014-3728-3

Ni, S., Ju, Y., Hou, Q., Wang, S., Liu, Q., Wu, Y., et al. (2009). Enrichment of heavy metal elements and their adsorption on ironoxides during carbonate rock weathering process. *Prog. Nat. Sci.* 19, 1133–1139. doi:10.1016/j.pnsc.2009.01.008

Parkhurst, D. L., and Appelo, C. A. J. (2011). User's guide to PHREEQC (Version2)-A computer Program for speciation, reaction path, advective transport, and inverse geochemical calculation. *U.S.Geological Surv. Water Resour. Investig.* doi:10.3133/wri994259

Pu, J., Cao, M., Zhang, Y., Yuan, D., and Zhao, H. (2014). Hydrochemical indications of human impact on karst groundwater in a subtropical karst area, Chongqing, China. *Environ. Earth Sci.* 72, 1683–1695. doi:10.1007/s12665-014-3073-4

Pu, J. B., Yuan, D. X., Jiang, Y. J., Guo, P. F., and Jian, J. Y. (2010). Hydrogeochemistry and environmental meaning of Chongqing subterranean karst streams in China. *Adv. Water Sci.* 21 (05), 628–636.

Pu, T., He, Y. Q., Zhang, T., Wu, J. K., Zhu, G. F., and Chang, L. (2013). Isotopic and geochemical evolution of ground and river waters in a karst dominated geological setting: a case study from Lijiang basin, South-Asia monsoon region. *Appl. Geochem.* 33 (33), 199–212. doi:10.1016/j.apgeochem.2013.02.013

Qiao, X. J., Hou, Q. L., Ju, Y. W., Liu, K., Zhang, Y. X., and Guo, G. X. (2014). Research about the control of geological structure on karst groundwater system in Zhangfang, Beijing. *Carsologica Sin.* 33, 184–191.

Rose, S. (2007). The effects of urbanization on the hydrochemistry of base flow within the Chattahoochee River Basin (Georgia, USA). *J. Hydrology* 341, 42–54. doi:10.1016/j.jhydrol.2007.04.019

Shand, P., Darbyshire, D. P. F., Love, A. J., and Edmunds, W. M. (2009). Sr isotopes in natural waters: applications to source characterisation and water-rock interaction in contrasting landscapes. *Appl. Geochem.* 24, 574–586. doi:10.1016/j.apgeochem.2008.12.011

Shen, Z. L. (1993). *Basis of hydrogeochemistry*. Beijing (BJ): Geology Publishing House. (in Chinese).

Shu, L. C., Zhou, Z. K., Li, F. L., Wu, P. P., Chen, H. W., and Xu, Z. X. (2020). Laboratory and numerical simulations of spatio-temporal variability of water exchange between the fissures and conduits in a karstic aquifer. *J. Hydrology* 590, 125219. doi:10.1016/j.jhydrol.2020.125219

Tao, J., Zhang, C., Ma, C., Yang, K., and Zhou, H. (2006). Geochemistry and petrogenesis of cretaceous high Sr and low Y granodiorite pluton in fangshan area, beijing. *Geol. Sci. Technol. Inf.* 25, 11–18. doi:10.3969/j.issn.1000-7849.2006.02.002

Valdes, D., Dupont, J.-P., Laignel, B., Ogier, S., Leboulanger, T., and Mahler, B. J. (2007). A spatial analysis of structural controls on Karst groundwater geochemistry at a regional scale. *J. Hydrology* 340, 244–255. doi:10.1016/j.jhydrol.2007.04.014

Wan, L., Jiang, X. W., and Wang, X. S. (2010). A common regularity of aquifers: the decay in hydraulic conductivity with depth. *Geol. J. China Univ.* 16 (1), 7–12. (in Chinese with English abstract). doi:10.16108/j.issn1006-7493.2010.01.006

Wang, X., Yang, L., Xu, H., and Ou, Z. (2016). Study on united regulation-storage of the Zhangfang karst grounwater reservoir in Beijing. *URBAN Geol.* 11, 26–29. (in Chinese with English abstract). doi:10.3969/j.issn.1007-1903.2016.01.006

Wang, X. G., and Jia, Z. X. (2007). *Joint Mapping and Its Applications* (China: China Institute of Water Resources and Hydropower Research).

White, W. B. (1988). *Geomorphology and hydrology of karst terrains*, 464. New York: Oxford University Press.

Winter, H., Stoll, J., and Aulbach, E. (1991). New electrical potential logging tool. *Sci. Drill.* 2 (4), 147–159. doi:10.1016/0148-9062(92)90760-W

Xie, Z. H., Zhang, Z. J., and Xing, G. Z. (2007). Analysis of the groundwater-supplySecurityabout the representative cities in NorthNorth China plain. *Resour. Sci.* 31 (3), 400–405. (in Chinese with English abstract). doi:10.3321/j.issn:1007-7588.2009.03.008

Xin, B. (2005). Hydrogeological characteristics of karst groundwater in fangshan district, beijing. *Geol. and Eng. Geol.*, 74–75. doi:10.3969/j.issn.1000-3665.2005.03.019

Yang, N., Li, S., Sun, Y., Zhang, Y., Xu, M., and Huang, Y. (2014). Study on characteristics of joints and fissures in karst region of Fangshan. *Beiing. Urban Geol.* 9, 30–32. (in Chinese with English abstract). doi:10.3969/j.issn.1007-1903.2014.01.008

Ye, C., Li, Y., and Tian, M. Y. (2005). Discuss on the potential of groundwater recharge based on GIS. *Hydrogeology and Eng. Geol.* 1, 67–69. (in Chinese with English abstract). doi:10.3969/j.issn.1000-3665.2005.01.016

Yidana, S. M., and Yidana, A. (2010). Assessing water quality using water quality index and multivariate analysis. *Environ. Earth Sci.* 59, 1461–1473. doi:10.1007/s12665-009-0132-3

Yu, J. C., Mo, X. X., Yu, X. H., Dong, G. C., Fu, Q., and Xing, F. C. (2012). Geochemical characteristics and petrogenesis of Permian basaltic rocks in Keping area, Western Tarim basin: a record of plume-lithosphere interaction. *J. Earth Sci.* 23, 442–454. doi:10.1007/s12583-012-0267-0

Zang, H. F., Jia, Z. X., and Zheng, X. Q. (2013). Characteristics of hydrochemical and carbon - sulfur isotopic for karst water in Liulin spring area. *Water Resour. Power* 31 (12), 28–32.